Two Tarantula Peptides Inhibit Activation of Multiple Sodium Channels[†]

Richard E. Middleton,[‡,§] Vivien A. Warren,[‡,§] Richard L. Kraus,[||] Jeremy C. Hwang,[§] Chou J. Liu,[§] Ge Dai,[§]
Richard M. Brochu,[§] Martin G. Kohler,[§] Ying-Duo Gao,[⊥] Victor M. Garsky,[#] Michael J. Bogusky,[#] John T. Mehl,[#]
Charles J. Cohen,[||] and McHardy M. Smith*,[§]

*Department of Ion Channels, Merck Research Laboratories, Rahway, New Jersey, Department of Membrane Biophysics and
Biochemistry, Merck Research Laboratories, San Diego, California, Department of Medicinal Chemistry, Merck Research
Laboratories, West Point, Pennsylvania, and Rahway, New Jersey, and Department of Molecular Systems, Merck Research
Laboratories, Rahway, New Jersey*

ABSTRACT: Two peptides, ProTx-I and ProTx-II, from the venom of the tarantula *Thrixopelma pruriens*, have been isolated and characterized. These peptides were purified on the basis of their ability to reversibly inhibit the tetrodotoxin-resistant Na channel, Na_V 1.8, and are shown to belong to the inhibitory cystine knot (ICK) family of peptide toxins interacting with voltage-gated ion channels. The family has several hallmarks: cystine bridge connectivity, mechanism of channel inhibition, and promiscuity across channels within and across channel families. The cystine bridge connectivity of ProTx-II is very similar to that of other members of this family, i.e., C_2 to C_{16}, C_9 to C_{21}, and C_{15} to C_{25}. These peptides are the first high-affinity ligands for tetrodotoxin-resistant peripheral nerve Na_V channels, but also inhibit other Na_V channels (IC_{50}'s < 100 nM). ProTx-I and ProTx-II shift the voltage dependence of activation of Na_V 1.5 to more positive voltages, similar to other gating-modifier ICK family members. ProTx-I also shifts the voltage dependence of activation of Ca_V 3.1 (α_{1G}, T-type, IC_{50} = 50 nM) without affecting the voltage dependence of inactivation. To enable further structural and functional studies, synthetic ProTx-II was made; it adopts the same structure and has the same functional properties as the native peptide. Synthetic ProTx-I was also made and exhibits the same potency as the native peptide. Synthetic ProTx-I, but not ProTx-II, also inhibits K_V 2.1 channels with 10-fold less potency than its potency on Na_V channels. These peptides represent novel tools for exploring the gating mechanisms of several Na_V and Ca_V channels.

Peptides that target voltage-gated Na channels are widely found in the venoms of scorpions, cone snails and sea anemones. Many have proven to be valuable tools for elucidating the structure, function, and physiology of the various Na_V[1] channel isoforms. Three classes of peptide toxins have been described (*1*): (A) site 1 toxins, e.g., the μ-conotoxins, bind to the pore of the channel and physically occlude the conduction pathway (*2−4*); (B) site 3 toxins, including the α-scorpion toxins, some sea anemone toxins and δ-conotoxins, bind to the S3−S4 linker of domain IV and slow channel inactivation (*5−7*); and (C) site 4 toxins, including the β-scorpion toxins, bind to the S3−S4 linker in domain II and facilitate channel activation (*8*). Both the site 3 and site 4 families of peptides, under defined conditions, increase the open probability of Na_V channels and inhibit gating transitions into closed states; they are therefore called "gating-modifiers". The gating modification can either inhibit deactivation (β-scorpion toxins) or inhibit the movement into the fast-inactivated state (e.g., α-scorpion toxins, *1*).

Spider venoms contain many peptide toxins that target voltage-gated ion channels, but almost all of the peptides that have been isolated target K_V or Ca_V channels (*9*). A number of these peptides are gating modifiers that conform to the inhibitory cystine knot (ICK) structural motif (*10*, *11*), which is a subset of the disulfide β-cross cluster of proteins (*12*). Some ICK peptides, such as the μ- and some ω-conotoxins, are thought to block the channel pore, while ICK peptides from spider venoms, such as hanatoxin1 and ω-Aga-IVA, bind to an S3−S4 linker domain of either K_V or Ca_V channels, respectively (*13−17*). In contrast to scorpion and sea anemone toxins, these spider toxins do not effect the rate of inactivation but inhibit channel activity by restricting the movement of the voltage sensor into the open channel

* Corresponding author. Address: P.O. Box 2000, RY80N-C31, Rahway, NJ 07065. Tel: 732-594-7013. FAX: 732-594-3925. E-mail: mchardy_smith@merck.com.

[‡] R.E.M. and V.A.W. contributed equally to this work and are listed alphabetically.

[§] Department of Ion Channels, Rahway.

[||] Department of Membrane Biophysics and Biochemistry, San Diego.

[⊥] Department of Molecular Systems, Rahway.

[#] Department of Medicinal Chemistry, West Point, PA, and Rahway, NJ.

[1] Abbreviations: BAPTA, 1,2-bis(2-aminophenoxy)ethane-*N,N,N',N'*-tetraacetic acid; Ca_V, K_V, and Na_V, voltage-dependent calcium, potassium, and sodium channels; FRET, fluorescence resonance energy transfer; HEPES, *N*-(2-hydroxyethyl)piperazine-*N'*-(2-ethanesulfonic acid); ICK, inhibitory cystine knot; LC-MS, liquid chromatography−mass spectrometry; MALDI-PSD, matrix-assisted-laser-desorption−ionization post-source decay; MALDI-TOF-MS, matrix-assisted-laser-desorption−ionization time-of-flight mass spectrometry; NOE, nuclear Overhauser effect; NOESY, nuclear Overhauser effect spectroscopy; PTH, phenyl thiohydantoin; RCM'ed, reduced and carboxymethylated; TCEP, tris(2-carboxyethyl)phosphine; TFA, trifluoroacetic acid; TOCSY, total correlational spectroscopy; TTX, tetrodotoxin.

conformation (shifting the voltage dependence of activation to more positive potentials). Many of these gating modifier spider toxins are promiscuous: ScTx1 blocks K$_V$ 2.1, 2.2, and 4.2, all with IC$_{50}$ values below 25 nM (*18*), and hanatoxin1 and grammotoxin block both K$_V$ 2.1 channels and Ca$_V$ 2.1 channels (*19*). Thus, the hallmarks of the ICK family of spider toxin gating modifiers are disulfide bridge connectivity, mechanism of channel inhibition, and promiscuity within and across voltage-gated ion channel families.

Here we report on the identification, purification, structural elucidation, and initial electrophysiological characterization of two peptides isolated from the venom of the tarantula, *Thrixopelma pruriens*. ProTx-I (35 amino acids)[2] completely conforms, and ProTx-II (30 amino acids) mostly conforms to the ICK structural motif. ProTx-I contains the same number of residues and the same cys spacing as hanatoxin1. ProTx-II possesses the same disulfide bridging connectivity as other members of the ICK class and can be chemically synthesized and folded to an active form. ProTx-II then expands the ICK motif in that it has only three residues between the fifth and sixth half-cystines, which is smaller than the spacing definition of 4−11 residues previously described (*11*). Both ProTx-I and ProTx-II behave as gating modifiers and inhibit the activation of Na$_V$ channels without affecting the inactivation process. This property has not previously been described with other peptide toxins that target Na$_V$ channels. ProTx-I and ProTx-II inhibit several Na$_V$ and Ca$_V$ channel isoforms and likely identify conserved structures in the voltage-sensing domains of both channel types. Preliminary reports of some of this work have been presented in abstract form (*20−22*).

MATERIALS AND METHODS

Materials. Venoms were purchased from commercial vendors. *Thrixopelma pruriens* tarantula venom was first purchased from Invertebrate Biologics, (Los Gatos, CA); more recent purchases were from Spider Pharm (Yarnell, AZ). This spider was originally identified as *Proshapalopus anomalous*, and we had published several abstracts using that name (*20−22*), but the tarantula was reclassified as *Thrixopelma pruriens* (*23*). Endoproteinases Arg-C, Lys-C, Glu-C, Asp-N, and sequencing-grade Trypsin were purchased from Roche Diagnostics Corporation/Boehringer Mannheim (Indianapolis, IN). Brevetoxin (PbTx$_3$) was from CalBiochem (San Diego, CA). Tris(2-carboxyethyl)phosphine (TCEP) was supplied by Pierce.

Toxin Purification. Venom aliquots were fractionated by cation exchange chromatography followed by reverse phase chromatography using C8, C4, and C18 columns. The high-pressure liquid chromatography (HPLC) systems and the data collection system were previously described (*24*). Aliquots of the *Thrixopelma pruriens* venom, up to 500 μL, were thawed and diluted 10-fold with 20 mM ammonium acetate, pH 6.2. The sample was then loaded onto a Brownlee CX-300 column (4.6 × 220 mm) at a flow rate of 1 mL/min. The column was run using distilled deionized water as solvent A and 1 M ammonium acetate at pH 6.2 as solvent B and had been preequilibrated at 2% B. Four minutes after

the final sample injection, material bound to the column was eluted using a gradient of 1.73% B/min. Absorbance at 280 nm was monitored, and peak fractions were collected. Fractions were lyophilized and reconstituted in 140 mM KCl, 10 mM HEPES−K, pH 7.4, and assayed for inhibition of Na$_V$ 1.8. Selected fractions were pooled and subjected to reverse-phase HPLC (C8, 4.6 × 250 mm, Vydac, Hesperia, CA) using 10 mM trifluoroacetic acid (TFA) in water (solvent A) and 9 mM TFA in 95% 2-propanol:5% water (solvent B). Sample was loaded at 10% B, and then a gradient of 10−50% B over 51 min at 1.25 mL/min flow rate was used to elute proteins. Absorbance was monitored at 220 nm. Fractions were lyophilized, resuspended, and assayed as above. The third stage C4 column (4.6 × 250 mm, Vydac) was run using 0.1% heptafluorobutyric acid in water (solvent A) and 0.1% heptafluorobutyric acid in 95% acetonitrile: water (solvent B). Active fractions were pooled, injected at 20% B, and eluted with a gradient of 20−45% B over 54 min at a flow rate of 1.25 mL/min. After lyophilization and electrophysiological analysis, active fractions were pooled and loaded onto a C18 column (4.6 × 250 mm, Vydac) with 10 mM TFA in water as solvent A and 9 mM TFA in 95% acetonitrile:water as solvent B. Material was eluted with a gradient of 18−43% B over 54 min at a flow rate of 1.2 mL/min; absorbance at 210 nm was monitored.

Protein Chemistry. The procedure for reduction and alkylation of peptides has been previously described (*24*). Purified proteins or peptide fragments were analyzed by automated Edman degradation chemistry using either a Porton 2090E microsequencer or an ABI Procise 494 cLC, operated according to the manufacturers' protocols; PTH-amino acid quantitation was carried out using the software supplied by the manufacturer. The Porton 2090E had been retrofitted with a diode array detector, and the signal at 268 nm (4 nm band-pass) was divided by the signal at 315 nm (25 nm band-pass). Quantitation of peptide was done by assuming that the initial yield of the sequencer was 50%, which was within 5% of the initial yield of the standards supplied by the manufacturers: α-lactoglobulin (Porton 2090E) or β-lactoglobulin (Procise 494 cLC).

For disulfide bridge determination, 2−10 nmol of ProTx-II was resuspended in 40 μL of 0.1 M Tris·HCl, pH 7.5, 5% acetonitrile, and digested at a 1:5 weight ratio with modified sequencing grade trypsin (Roche Diagnostics GmbH, Mannheim, Ger.). The digestion proceeded for 48 or 120 h at 37 °C for the 2 and 10 nmol digests, respectively. The digested material was separated on an ABI microbore HPLC; solvent A was 5 mM TFA in water, and solvent B was 4.5 mM TFA in 95% acetonitrile:water (*24*). Material was eluted at 100 μL/min using a gradient of 5−55% B over 56 min at 35 °C (C18 column, 2.5 × 150 mm, Vydac) and following absorbance at 205 and 280 nm; two major and one minor component were observed and separately collected. The major components were subsequently lyophilized and digested with 3.86 μg endoproteinase Glu-C in 50 μL of 25 mM NH$_5$CO$_3$, pH 7.8, 5% acetonitrile for 18 h at 25 °C, and were purified as above. When the trypsin digestion was carried out on either the native or the synthetic material at pH 8.5, significant disulfide bridge scrambling was found: e.g., C$_2$ was found bridged to C$_9$, to C$_{25}$ and to C$_{15}$−C$_{21}$ in similar amounts. At pH 7.5, however, undetectable amounts

---

[2] The protein sequence data reported in this paper will appear in the SWISS-PROT and TrEMBL knowledgebase under accession numbers P83480 and P83476 for ProTx-I and ProTx-II, respectively.

(<3%) of C_2 to C_9 or to C_{25} forms were found with either the native or the synthetic ProTx-II.

For primary sequence determination, 500 pmol samples of the reduced and carboxymethylated (RCM'ed) peptides were resuspended in the appropriate reaction buffer for a given cleavage enzyme. The reaction with 5 pmol of endoproteinase Lys-C was carried out in 50 μL 0.1 M NH$_5$-CO$_3$ for 16 h at 37 °C. Digestion by 5 pmol of endoproteinase Asp-N was performed under the same conditions for 18 h. Endoproteinase Arg-C was used at 0.3 μg enzyme per 108 pmol of the toxin in 50 μL of 50 mM Na$_2$HPO$_4$, 4 mM CaCl$_2$, at pH 7.9. Just prior to fragment separation by reverse-phase chromatography, TFA was added to a final concentration of 1%, and the samples were fractionated as above.

Mass Spectrometry. Matrix-assisted-laser-desorption−ionization time-of-flight mass spectrometry (MALDI-TOF-MS) was used for structural characterization of the fractions to determine mass and to estimate purity. MALDI-TOF-MS and MALDI-PSD measurements were performed using a Voyager-DE STR reflectron time-of-flight mass spectrometer from Applied Biosystems (Framingham, MA). In cases where an HPLC was used to separate components, fractions containing 1−5 pmol of sample were lyophilized. Fractions were then reconstituted in 2 μL of matrix solution (10 mg/mL α-cyano-4-hydroxycinnamic acid in 70% acetonitrile/0.1% TFA). One microliter of sample/matrix solution was deposited and dried under a gentle stream of warm air. In cases where an HPLC fraction was not used, a C-18 ZipTip from Millipore (Milford, MA) was used for purification. After loading the sample onto the ZipTip and washing, the sample was eluted off the ZipTip column using 2 μL matrix solution. Typically, 100−500 laser shots were averaged into a composite spectrum. For MALDI-PSD measurements, the parent ion is selected using the precursor ion-gate. The PSD spectrum was acquired by scanning the reflectron mirror ratio. At each mirror ratio setting between 800 and 1200 laser shots are averaged using high laser intensity. The final PSD spectrum is generated by stitching the PSD segments together using the Data Explorer software module (Applied Biosystems).

LC-MS was performed on intact ProTx peptides to confirm molecular weight and purity using a TSQ-7000 triple quadrupole mass spectrometer Finnigan Mat (San Jose, CA) configured with an electrospray ionization source. The mass spectrometer was connected to an 1100 Series HPLC from Agilent (Palo Alto, CA). A 2.0 × 50 mm PLRP-S column from Michrom BioResources (Auburn, CA) was used. Samples were loaded onto the column using 100% solvent A (5% acetonitrile/0.05% TFA) and isocratically eluted using 80% solvent B (acetonitrile/0.05% TFA). The flow rate was 200 μL/min, and no splitter was used prior to the mass spectrometer. The tools used to calculate molecular masses were either www.expasy.org/tools/peptide-mass.html, with corrections for the oxidation state of cys residues and for addition of water at any peptide backbone cleavages, or the Data Explorer software supplied by the manufacturer.

Peptide Synthesis. ProTx-I and ProTx-II were synthesized by solid-phase methodology using a Boc protection strategy (*25*). Folding of HPLC purified hexahydropeptides was achieved by air oxidation (0.1 mg/mL) in 2 M urea, 0.1 M Tris, pH 8.0, 0.15 mM reduced glutathione, and 0.30 mM oxidized glutathione. The yield of the folding reaction was 77% for ProTx-II and >70% for ProTx-I, and the overall yield of the synthesis to folded toxin was 1%.

NMR Spectroscopy. All NMR spectra were recorded on a Varian Inova 600 MHz spectrometer with a sample temperature of 25 °C. Samples for NMR measurements contained 1.02 mg of the synthetic folded ProTx-II peptide dissolved in 50 mM sodium phosphate buffer in 90% H$_2$O/10% D$_2$O, pH 5.73 in a volume of 0.650 mL. ^{1}H chemical shifts were referenced internally to sodium 3-(trimethylsilyl)propionate-2,2,3,3-d$_4$ (TSP) at 0.00 ppm. The water resonance in all experiments was suppressed by low power saturation using an attenuated transmitter pulse. Sequence-specific ^{1}H chemical shift assignments were obtained with the combination of TOCSY (*26, 27*) and NOESY (*28*) experiments using standard methodologies (*29*). All two-dimensional experiments were acquired in the hypercomplex mode for phase-sensitive presentation (*30*). Clean-TOCSY (*27, 31*) spectra were recorded with 1K complex points in t_2 and 512 points in t_1 consisting of 64−96 transients per increment. Spin-locking was achieved with an MLEV16+60° mixing sequence for a duration of 65 ms preceded by a 2.0 ms trim pulse. Data sets were multiplied by a shifted Gaussian apodization function and zero-filled to 2K by 1K complex points prior to Fourier transformation.

NOESY spectra were acquired using mixing times of 250 and 500 ms. Solvent suppression was achieved by selective saturation of the water resonance during the 1 s recycle delay, t_1 period, and mixing period. Data sets were acquired with 1K complex points in t_2 and 512 points in t_1 with 96 transients per increment. The data were processed as described above. The sample was lyophilized and redissolved in 100% D$_2$O for additional assignment and analysis of resonances near the H$_2$O peak. There was negligible perturbation of the chemical shift values recorded on the peptide samples dissolved in D$_2$O.

rNa$_V$ 1.8 Cloning and Oocyte Electrophysiology. RNA from 100 dorsal root ganglia (20 day-old Wistar rats, Charles River Laboratories) was prepared with the Trizol Method (Gibco BRL). RNA was reverse transcribed with random primers and Superscript II reverse transcriptase (Gibco BRL). rNa$_V$ 1.8 specific sequences were amplified with primers according to published sequences of rNa$_V$ 1.8 (*32*). For the PCR, Advantage polymerase (Clontech) was used. Two independent fragments were amplified with CGATGCTAG-CAAGCTTCCGCCACCATGGAGCTCCCCTTTGCGT-CCGTGG and CATATCTTCCTCGAGCTCGTCGAGGT-CAGATTCC and with GGAATCTGACCTCGACGAGCTC-GAGGAAGATATG and GCATTCTAGAGCCTGAGTGC-CTTCACTGAGGTCCAGGGCTG. The PCR fragments were digested with restriction enzymes and cloned in plasmid vectors. Several inserts containing plasmids for each fragment were sequenced. Sequence differences from the published sequence were A59D, A88T, A432E, L572V, and D588H. The full length rNa$_V$ 1.8 cDNA was assembled in pSK from Stratagene.

To express channels in oocytes, cDNA encoding the appropriate channel was cloned into standard expression vectors except for hNa$_V$ 1.7 and rNa$_V$ 1.8, which were cloned into a modified pGEM vector (Promega) containing the *Xenopus* β-globin 5′ and 3′ untranslated region to enhance expression levels (*33*). Plasmids were linearized, and RNA was transcribed using the T7 (or SP6) RNA polymerase and

the mMessage mMachine kit from Ambion. Undiluted RNA was injected for the hNa$_V$ 1.7 (h for human), and rNa$_V$ 1.8 (r for rat) channels but was diluted for all other channels to obtain maximum current amplitudes of between 0.5 and 5 μA at test potentials 2−7 days after mRNA injection. Current amplitude was measured using a Dagan two-electrode voltage-clamp amplifier and the pCLAMP acquisition software. Leak current was subtracted using the scaled current observed with a P/n protocol. The capacitance and resistance compensation feature on the Dagan was used to minimize the capacitance transient measured at a voltage where Na$_V$ channels were not opened. Glass microelectrodes were pulled to achieve resistances of 0.5−1.0 MΩ after filling with 1 M KCl measured in the recording solution. Oocytes were prepared by standard techniques and recording done in ND-96 (98 mM NaCl, 2 mM KCl, 1 mM MgCl$_2$, 1.5 mM CaCl$_2$, 5 mM HEPES−Na, pH 7.5). Oocyte membrane potential was held at −80 or −100 mV, and a current−voltage relationship was measured to determine the voltage that produced the maximum inward current. Typically, oocytes were depolarized to 0 mV (+ 20 to + 30 mV for rNa$_V$ 1.8) for 40−100 ms. After a stable peak current was obtained, the indicated concentration of venom or toxin was added by perfusing the 1 mL recording chamber with ND 96 containing the sample, typically at 2−3 mL/min. When a stable block was obtained ($\approx$15 min), the oocyte was perfused with fresh ND-96 to assess reversibility of inhibition.

Cell Culture and HEK Cell Electrophysiology. For whole-cell voltage-clamp recordings, stably transfected HEK-293 cell lines expressing hNa$_V$ 1.5 (*34*), hNa$_V$ 1.7 (see below *35*), or rCa$_V$ 3.1 (*36*) channels were used. The hNa$_V$ 1.7 cell line was constructed by Aurora Biosciences. The hNa$_V$ 1.7 cDNA (*35*) was cloned in a retroviral expression vector (pLCNX, Clontech). Subsequently virus particles were used to infect HEK-293 cells, and a cell line stably expressing the channel was selected. Cells were maintained in either MEM (Minimum Essential Medium) supplemented with 10% fetal bovine serum, 2 mM L-glutamine, 1 unit/mL penicillin/ streptomycin or DMEM (Dulbecco's modified Eagles medium) supplemented with 10% fetal bovine serum, 4 mM L-glutamine, 2 units/mL penicillin/streptomycin, 0.02 mg/ mL G-418, as appropriate. Cells were plated on poly-D-lysine coated cover slips 16 h prior to recording then washed with mammalian Ringer's solution immediately prior to recording.

Single cell recordings of currents through voltage-activated hNa$_V$ 1.5, hNa$_V$ 1.7, and rCa$_V$ 3.1 channels were performed at room temperature (20−22 °C) using the whole cell patch-clamp technique. Currents were recorded using a Dagan 3900A or HEKA EPC-9 patch clamp amplifier. Data were stored on a personal computer equipped with HEKA Pulse 8.5 and analyzed using Pulsefit (HEKA, Lambrecht, Germany), Igor Pro 4.0 (Wavemetrics, Lake Oswego, OR), or Origin 6.0 (Microcal, Northampton, MA). Patch pipets were made from borosilicate glass tubing (World Precision Instruments, Sarasota, FL), fire-polished, and coated with Sylgard and had a resistance of 1−3 MΩ when filled with an internal solution (below) measured in the recording medium. Series resistance was compensated. Leak resistance and capacitance were corrected by subtracting the scaled current observed with a P/n protocol. For sodium current measurements, the following solutions were used (in mM), as stated in figure
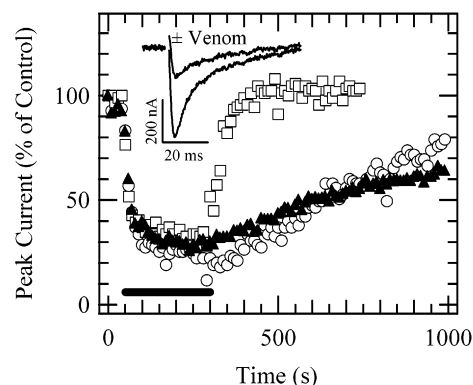

FIGURE 1: Effects of *Thrixopelma pruriens* venom and purified ProTx-I and ProTx-II on rNa$_V$ 1.8 expressed in oocytes. The membrane potential was held at −80 mV, and the peak inward current was measured during a 100 ms pulse to +30 mV, repeated every 10 s. During the recording, oocytes were perfused with a solution of ND-96 containing 1:2000 dilution of venom (▲), 730 nM ProTx-I (○), or 797 nM ProTx-II (□). These solutions were applied during the period indicated by the bar; all other times, the recording chamber was perfused with ND-96. The inset shows two-electrode voltage-clamp of oocytes expressing rNa$_V$ 1.8 recorded in ND-96; the current observed before and after application of a 1:2000 dilution of *Thrixopelma pruriens* venom is depicted.

legends: (pipet solution a) 2 NaCl, 101 Cs·gluconate, 20 CsF, 20 CsCl, 11 BAPTA, pH 7.4 adjusted with CsOH or (pipet solution b) 140 CsF, 10 NaCl, 1 EGTA, 10 HEPES, pH 7.3 adjusted with CsOH; and (bath solution a) 15 NaCl, 135 N-methyl-D-glucamine-Cl, 1.8 CaCl$_2$, 0.5 MgCl$_2$, pH 7.4 with HEPES or (bath solution b) 15 NaCl, 135 choline-Cl, 1 MgCl$_2$, 10 HEPES, pH 7.3 adjusted with TEA-OH. For calcium current measurements, the pipet solution contained 100 Na-glutamate, 20 CsF, 20 CsCl, 11 BAPTA, 10 HEPES, pH 7.2, and the bath solution consisted of 144 CsCl, 2 CaCl$_2$, 0.5 MgCl$_2$, 10 HEPES, pH 7.4. Purified or synthetic peptides were dissolved in 100 mM KCl and 10 mM HEPES−K, pH 7.5, stored at −20 °C, and diluted in the bath solution containing 0.05% BSA (essentially fatty acid free, Sigma, St. Louis, MO) to prevent adsorption of the peptide to tubing and perfusion chamber. Data are given as mean ± standard error.

VIPR Assay. hNa$_V$ 1.7 or hNa$_V$ 1.5 cells were plated at approximately 100 000 cells/well in poly-D-lysine coated black-wall clear-bottom 96 well plates (Costar # 3667) and were incubated overnight at 37 °C in a 10% CO$_2$ atmosphere in growth medium. Cells were stained with voltage-sensitive dyes (*37*, *38*) by washing twice with 100 μL of Dulbecco's phosphate buffered saline (DPBS) and then incubating in 100 μL of the DPBS supplemented to 10 mM glucose, 10 mM HEPES−Na (pH 7.5), and 10 μM CC2-DMPE for 0.7 h at 27 °C. Cells were rinsed twice with 100 μL of Na-free medium (in mM: 160 tetramethylammonium·Cl, 0.1 CaCl$_2$, 1 MgCl$_2$, 11 glucose, 10 HEPES−K, pH 7.5, [K] approximately 4.5 mM) and then incubated in 100 μL of that medium supplemented with 10 μM DiSBAC$_2$(3), 20 μM veratridine, 20 nM PbTx$_3$, and test sample at the indicated concentration for 0.7 h at 27 °C. At the end of this incubation, the plate was placed in the VIPR reader, illuminated at 400 nm, and fluorescence emissions at 460 and 580 nm were recorded at 1 Hz. After a 7 s baseline reading, 100 μL of Na solution was added (in mM: 165 NaCl, 4.5 KCl, 2 CaCl$_2$, 1 MgCl$_2$, 11 glucose, 10 HEPES−Na, pH 7.5). The change
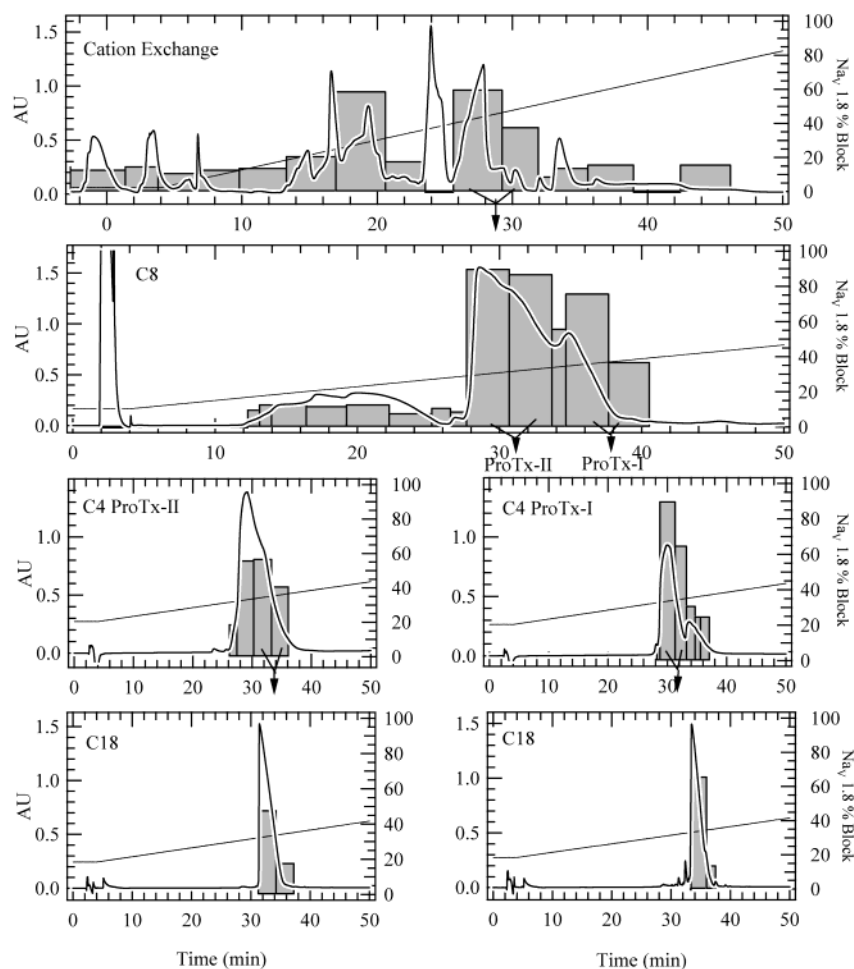
FIGURE 2: Purification of ProTx-I and ProTx-II. Top panel: venom (475 μL) was loaded onto a CX-300 cation exchange column. Proteins were eluted using a gradient from 20 mM to 1 M NH_5CO_3; the progress of the gradient is depicted with the straight line, plotted against the right-hand scale in units of % B. The absorbance of the eluent was measured at 280 nm (continuous trace, left scale). Fractions were analyzed for their capacity to inhibit Na current through rNa$_V$ 1.8 (bars, right scale). The indicated fractions were pooled and loaded onto a C8 column (next panel). Absorbance was monitored at 220 nm; fractions were tested as above. The indicated fractions were pooled and loaded onto two separate C4 runs, monitored at 210 nm, tested as above, and the indicated fractions from those runs were loaded onto two separate C18 runs (bottom panels), monitored at 210 nm. The fraction in front of the indicated C4 ProTx-II purification was also run on a C18 column and yielded ProTx-II by Edman degradation and by molecular mass (MALDI-TOF-MS).

in fluorescence resonance energy transfer (FRET) ratio was recorded as F/F_0 or more explicitly as

$$F/F_0 = ((S_{460}/S_{580})/(I_{460}/I_{580}))$$

where S and I are stimulated and initial fluorescence emissions measurements at the indicated wavelengths. The initial second through seventh readings were averaged for the denominator and the stimulated response was picked as the average of the 12th through the 15th readings. Background fluorescence ($\approx 16-20\%$ of the initial signal) was not subtracted.

RESULTS

Inhibition of current passing through rNa$_V$ 1.8 (rat PN3, SNS) channels expressed in *Xenopus* oocytes was used to screen over 125 spider, sea anemone, scorpion, and wasp venoms. *Thrixopelma pruriens* tarantula venom was identified as one of the most potent at inhibiting current movement through this channel. Addition of this venom caused a rapid, reproducible decrease in peak current of nearly 70%, which slowly reversed over a 15 min washout period (Figure 1,

triangles). To isolate the active agent(s), the venom was fractionated over a cation exchange column, and the fractions assayed for inhibition of rNa$_V$ 1.8 (Figure 2, top panel).

Two peaks of activity eluted, at about 20 and 28 min. The activity evident at 20 min is not discussed here, as it was present in much lower proportion in early batches of the venom. Two highly active fractions from the later eluting peak were pooled and fractionated over a C8 reverse-phase column (Figure 2, second panel). This sample separated into two peaks that eluted starting at 28 and 34 min. These two peaks of activity were distinguishable by the rate at which sodium channels recovered from block. Block of rNa$_V$ 1.8 reversed more rapidly by the fractions that would ultimately yield ProTx-II than by the fractions that would yield ProTx-I (Figure 1). These fractions were subsequently purified individually with two more reverse-phase purification steps prior to characterization by mass spectrometry and automated Edman sequencing.

The yield of ProTx-I and ProTx-II over the course of three purifications was not constant. From a single purification, the final yield was 1.1 μmol of ProTx-I and 0.8 μmol of ProTx-II per mL of venom, which indicates a high toxin

concentration. Other purifications yielded lower amounts: from 0.05 to 0.3 μmol of ProTx-I and ProTx-II per mL of venom. The differing yields may be due to the condition of the tarantulas, or seasonal variation in the venom.

The purity of the material recovered from the C18 column was assessed. Automated Edman degradation performed on native or reduced and carboxymethylated (RCM'ed) material revealed single sequences for both ProTx-I and ProTx-II (Figure 3, lower). On the basis of the sensitivity of the instruments, there were no positions in the first 20 residues at which multiple residues could be assigned, down to a 3% maximal possible impurity level. Following purification, ProTx-I and ProTx-II were analyzed by MS and found to contain only one peak, each at 3988 and 3827 amu, respectively (Figure 3, upper panels). By MS analysis, we estimate that greater than 97% of the signal was due to these species. When the material was injected into a new HPLC system, with a different column and gradient, <3% maximal impurities were detected by UV absorbance at 280 or 205 nm. Thus, by these three criteria, the material was >97% pure.

Sequences. Sequencing the RCM'ed material typically yielded about 30 cycles of identifiable amino acid residues and the phenylthiohydantoin carboxymethyl-cysteine derivatives (PTH CMCys) in the indicated cycles (Figure 3, lower). To confirm and extend these results, peptide fragments were generated with endoproteinases Lys-C, Arg-C, or Asp-N digestion of RCM'ed ProTx-I and ProTx-II or trypsin digestion of the native ProTx-II. All fragment sequences were consistent with the original full-length sequence and the critical fragments used for sequence determination are shown. To determine the C-terminal residues in ProTx-I and confirm the assignments in ProTx-II, peptides generated by Asp-N or trypsin digestion respectively were sequenced by MS/MS.

Disulfide Bridge Connectivity. The tertiary structure of hanatoxin1, determined by NMR (*39*), and the disulfide connectivity of huwentoxin-1, determined by peptide mapping (*40*), reveal the characteristic ICK disulfide pattern in which the first, second, and third half-cystines bridge to the fourth, fifth, and sixth half-cystines, respectively. ProTx-I is 57% identical to hanatoxin1 (*41*) and has the same cys spacing (Figure 3). The dihydroalanine PTH results from sequencing the native ProTx-I (below) suggests that ProTx-I is an ICK peptide. However, ProTx-II is only 10% identical to hanatoxin1 (excluding the cys residues) and is five residues shorter, including three residues missing between the 5th and 6th cys residues (Figure 3). With only three residues between the 5th and 6th cys residues, ProTx-II falls outside the definition of an ICK motif peptide (*11*). Therefore, we determined the disulfide bridge connectivity of ProTx-II by several techniques to determine if it is an ICK motif protein.

The masses of ProTx-I and ProTx-II measured by MALDI-TOF or electrospray were 3988.3 ± 0.58 (*n* = 3) and 3827.0 ± 0 (*n* = 2). If all cys residues were in disulfides, then the calculated masses, based on the sequences, are 3987.56 and 3826.64 amu, respectively (reduced would be 3993.56 and 3832.64 amu, respectively). When ProTx-II was reduced using TCEP, >85% of the molecules increased in mass by 6 amu (Figure 3, inset) consistent with three disulfide bonds. These results support the conclusion that all cys residues are in the form of disulfides.
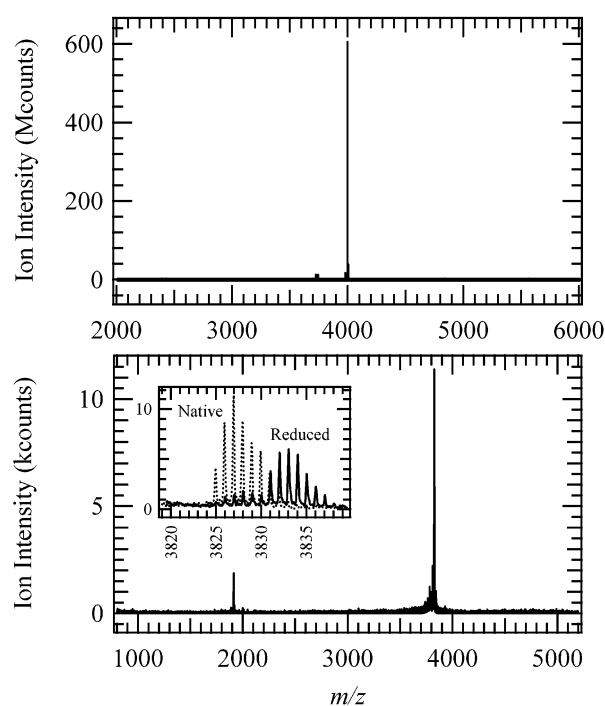


```
ProTx-I Primary Structure Determination
 Final ECRYWLGGCSAGQTCCKHLVCSRRHGWCVWDGTFS
Native EXRYWLGGXSAGQTXBKHLVBSXXHGWBVWDGT
RCM'ed ECRYWLGGCSAGQTCCKHLVCSRRHGWCVWD
 Lys-C ECRYWLGGCSAGQTCC HLVCSRRHGWCVWD
 Arg-C                        RHGWCVWDGTF
 Asp-N (MS/MS)                        DGTFS

ProTx-II Primary Structure Determination
  Final YCQKWMWTCDSERKCCEGMVCRLWCKKKLW
 Native YXQKWMWTXDSERKXBEGMVBRLWBKKKLw
 RCM'ed YCQKWMWTCDSERKCCEGMVCRLWCKKKLw
  Lys-C      WMWTCDSERKCCEGMVCRLWC
Trypsin (MS/MS & ProSeq)              KLW

Alignment with HaTx-1
ProTx-I  ECRYWLGGCSAGQTCCKHLVCSRRHGWCVWDGTFS
HaTx1    ECRYLFGGCKTTADCCKHLGCKFRDKYCAWDFTFS
ProTx-II YCQKWMWTCDSERKCCEGMVCRL···WCKKKLW··
```

FIGURE 3: Mass and amino acid sequence of ProTx-I and ProTx-II. Representative LC-MS of ProTx-I (top) and MALDI-TOF-MS spectra of ProTx-II (second); the inset in the ProTx-II panel shows MALDI-TOF of ProTx-II before and after reduction with TCEP. Reduction was carried out by lyophilizing a toxin aliquot and resuspending the toxin in 1 mg/mL TCEP in 100 mM NH$_5$CO$_3$ at room temperature for 1 h. In the ProTx-II panel, the second peak at 1914 is an *m*/2*z* peak as the isotope peaks were not separated by 1 amu (as are those in the inset) but were separated by 0.5 amu, and the isotopic ratio of the 1914 amu peaks matched that of the 3827 amu peaks. These panels are representative of the three ProTx-II or two ProTx-I separate isolations which generated independent samples. Lower panel: Sequences of native or reduced and carboxymethylated (RCM'ed) ProTx-I and ProTx-II, or peptide fragments from endoproteinase digestions of RCM'ed peptide. The lowercase letters are sequence calls with much reduced yield; the X for cycles where no PTH-amino acid derivative was identified, and the B is used to indicate cycles where the PTH derivative of dihydroalanine was seen in increased yield, not coincident with a serine. (N.B: The identification of the PTH-dihydroalanine was made only with samples sequenced on the Porton 2090E with the dual-wavelength detector; similar observations have not been found with the Procise 494 cLC, which uses a single-wavelength detector.) MS/MS refers to samples subject to MS/MS sequencing, and ProSeq refers to a sample that was subject to both MS/MS and automated Edman sequencing. In the final sequences, all residues were detected at positions at least twice except for the C-terminal serine in ProTx-I, which was identified only by MS/MS; for example, K$_{28}$ of ProTx-II was detected at least 6 times. Bottom panel: alignment of ProTx-I and ProTx-II with hanatoxin1 (HaTx1).
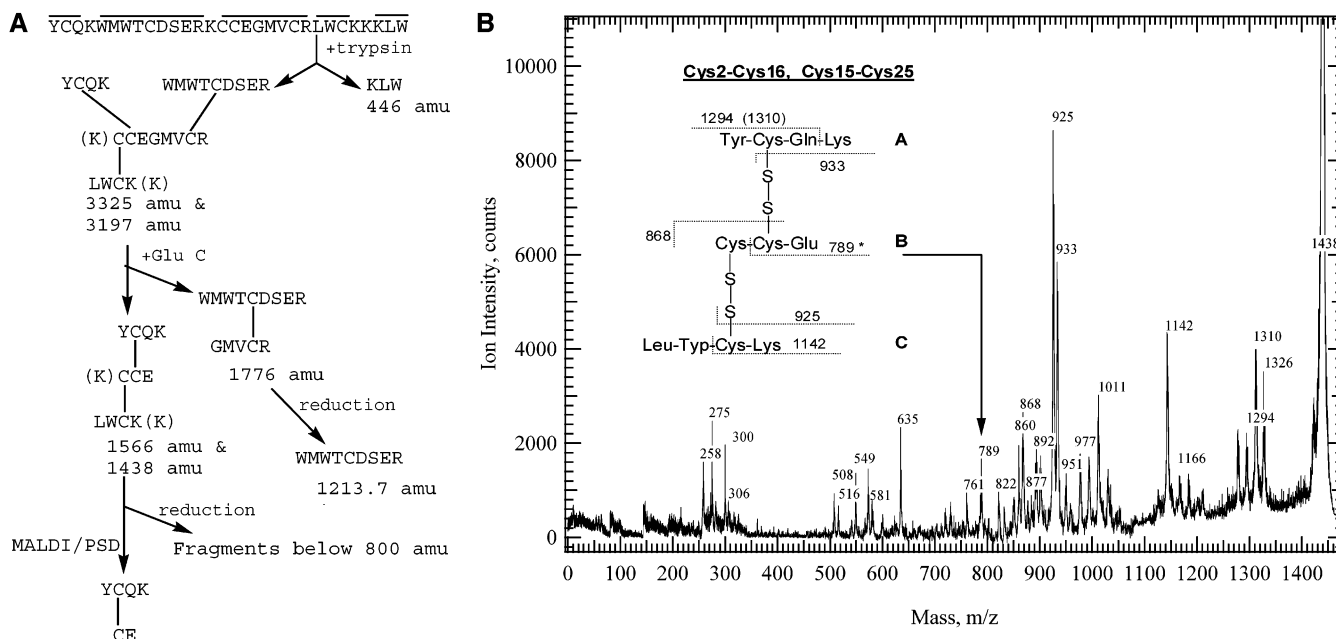
FIGURE 4: (A) Identifying the disulfide bridge connectivity of ProTx-II. The sequence of the intact sequence is shown at the top with overbars indicating the recovered trypsin fragments. Native ProTx-II was digested with trypsin, the products were separated by HPLC, and the peaks were subject to MALDI-TOF-MS and PTH-amino acid sequencing. A smaller peak eluting earlier, when subject to N-terminal amino acid sequencing, gave the sequence KLW; this material by MALDI-TOF-MS had a molecular mass of 446 (expected 445.56) and, when subject to MS/MS, also gave the sequence KLW. There was no indication of amidation of the W; the masses were exactly that expected for a carboxylic acid group at the carboxy terminus of the protein. The major product had a molecular mass of 3325.05 or 3325.53 (separate isolations), longer digestion times gave 3197 as the major species recovered. The expected masses were 3324.92 and 3196.75 amu based on the sequence, with the cys residues oxidized and the peptide backbone cleaved in three places by trypsin. When the 3197 amu species was subsequently digested with Glu-C, two products were separated by HPLC: a 1776 amu (calculated 1776.05 amu) and a 1438 amu species (calculated 1437.72 amu). Similarly, digestion of the 3325 amu species resulted in isolation of 1566.997 amu (calculated 1566.89 amu) and 1776.1 amu (calculated 1776.05 amu) species. If these products were reduced prior to MALDI-TOF, they disappeared, consistent with a disulfide bridge or bridges. In one case, the fragment containing C_9 was obtained at 1213.7 amu (calculated 1213.35 amu); the lower molecular mass fragments were not detected in increased signal intensity significantly above the matrix signal. Figure 4B is the MALDI-PSD spectrum of the HPLC fraction. The first digit is over the identified peak. The observed b-ions, y-ions, and other ions due to cleavage of the disulfide linkage confirm the structure of this proteolytic fragment (see Table 1). The peak at 789 *m/z* is critical for determining the bridging pattern as C_2C_{16} and $C_{15}C_{25}$. There is no peak observed at 798 *m/z*, 10 amu higher, which would have indicated the opposite disulfide bridging pattern.

Sequencing native ProTx-I and ProTx-II did not yield PTH−Cys derivatives in the cycles where cys was assigned, consistent with the cys residues being in the form of half-cystines (*40*). The native samples did yield PTH-dihydroalanine (*40*) in increased yield in cycles 16, 21, and 28 for ProTx-I and in cycles 16, 21, and 25 for ProTx-II (50−80% of the yield of the surrounding residues) relative to that seen in cycles 2, 9, and 15 (yield of 7−30% of the surrounding residues). This suggests that C_2, C_9, and C_{15} do not disulfide-bridge with each other, consistent with an ICK motif for both ProTx-I and ProTx-II.

To determine the specific disulfide connectivity of ProTx-II, protease digestion was employed (Figure 4A). Trypsin has potential cleavage sites between each cys residue except C_{15} and C_{21}. Trypsin digestion caused the native ProTx-II at 3827 amu to disappear while major products with masses of 3325.5 and 3197 amu and a minor 446 amu product appeared. The 446 amu species sequenced as KLW by MS/MS and automated Edman sequencing (Figures 3 and 4A). The presence of the 3325 and the 3197 amu species indicates that C_2, C_9, and C_{25} are bonded to the peptide containing $C_{15}C_{16}$ and C_{21}.

Glu-C cleaved the 3325 and the 3197 amu samples after E_{17}, and the digestion products were separated by HPLC. Three products with molecular masses of 1776, 1566, and 1438 amu were identified (Figure 4A). The 1438 amu was

exclusively derived from the 3197 amu Glu-C reaction, the 1556 amu species was exclusively derived from the digestion of the 3325 amu starting material, and the 1776 amu was common to both reactions. The 1776 amu peak yielded two sequences: the tryptic fragment starting with W_5 and the predicted Glu-C product starting at G_{18} (Figure 4A). When subject to MALDI-TOF-MS after reduction with TCEP, the 1776 amu disappeared, and a 1213 amu species appeared (Figure 4A). The 564 amu product was not observed and may have been lost after reduction. Thus, by Edman sequencing and by MS, we find direct evidence that C_9 is in a disulfide bridge with C_{21}, or the 2nd and 5th half-cystines bond to each other in a pattern consistent with the ICK motif.

The 1438 amu molecule, when sequenced, yielded Y and L in the first cycle, W in the 2nd cycle, E and Q in the 3rd cycle, and K in the 4th cycle (Figure 4A). The two sequences depicted in Figure 4A were observed from the 1566 amu material: about 30% of the sample had K_{14} and did not have K_{27}, while the remainder had K_{27} and no K_{14}. Therefore, C_2 and C_{25} must be attached to the fragment that contained C_{15} and C_{16}, and they cannot bond to each other. This pattern is consistent with the ICK disulfide bridging pattern where the 1st cys bonds to the 4th cys and the 3rd cys bonds to the 6th cys. On the basis of the dihydroalanine PTH data and the proteolytic cleavage data, this protein must conform to an ICK motif: the 1st cys cannot bond to the 6th cys (peptide

Table 1: Identification of Calculated and Observed Fragments Generated by MALDI-PSD Fragmentation of the 1438 amu (See Text and Figure 4B for Nomenclature)

structure	calc.	obs.	structure	calc.	obs.
Ab_2	1165.5	1166	A	540.7	541
Ab_3	1293.6	1294			
Ay_2	275.6	275	A(+S)	572.7	572
Ay_3	1276.6	1277	A(−S)	508.7	508
Bb_2	1291.7	1292	C	548.7	549
By_2	789.3	789	C(+S)	580.7	581
			C(−S)	516.8	516
Cb_2	300.4	300	A+B	892.1	892
Cb_3	1293.6	1294	A+B(+S)	924.1	925
Cy_2	1139.1	1142	A+B(−S)	860.1	860
Cy_3	1325.6	1326	B+C	900.2	900
			B+C(+S)	932.2	933
			B+C(−S)	868.2	868

mapping of the 1438), it cannot bond to the 2nd or 5th cys residues (peptide mapping), and it cannot bond to the 3rd cys (PTH dihydroalanine data); therefore, it must bond to the 4th cys. By elimination then, the 3rd cys and 6th cys must also form a bond.

MALDI-PSD Analysis of Disulfide Bridging Pattern. Mass spectrometry can be used for in situ fragmentation and analysis of peptides joined by disulfide bridges. MALDI-PSD has been shown to be advantageous to other forms of MS/MS analysis because the energetics of PSD can lead to fragmentation of the peptide backbone between adjacent half-cystine residues (*42*). Unique fragment ions are generated that contain the disulfide bridges and provide evidence for the assignment of the bridging patten. Figure 4B is a PSD spectrum of the proteolytic fragments from the parent ion of 1438 amu. There are a large number of a, b, and y ions formed by cleavage along the three peptide backbones, as well as fragment ions generated by cleavage of the disulfide bridges. Table 1 lists the observed ions along with assignments. For purposes of clarity, the peptide chains of the parent ion are labeled A, B, and C (inset, Figure 4B). The By_2 ion at 789 amu formed by cleavage of the B chain between C_{15} and C_{16} provides the critical information for assigning the disulfide bridging connectivity (Figure 4B and Table 1). This ion is only consistent with disulfide bridges between C_2–C_{16} and C_{15}–C_{25}. If the bridging pattern were the opposite, i.e., C_2–C_{15} and C_{16}–C_{25}, then an ion at 798 amu should have been observed, but it was absent. We conclude that ProTx-II does adopt an ICK motif.

Electrophysiological Studies. The effect of ProTx-I and ProTx-II on channel activation was studied using hNa_V 1.5 channels expressed in HEK-293 cells. Panels A and B of Figure 5 show superimposed hNa_V 1.5 currents without and with 365 nM ProTx-I for test potentials of −10 mV and +95 mV, respectively. The toxin effect is much greater for small depolarizations, with negligible block at +95 mV. The effect of ProTx-I on the peak current−voltage relationship is shown (Figure 5C). Note that the voltage of half-maximal activation is shifted by +37 mV and the slope factor is increased ≈2-fold. Similar results were obtained in two other experiments, but we were unable to resolve outward currents at very positive voltages and quantify the effect of toxin on the voltage dependence of activation. ProTx-II was tested on hNa_V 1.5 also and was found to have a similar efficacy
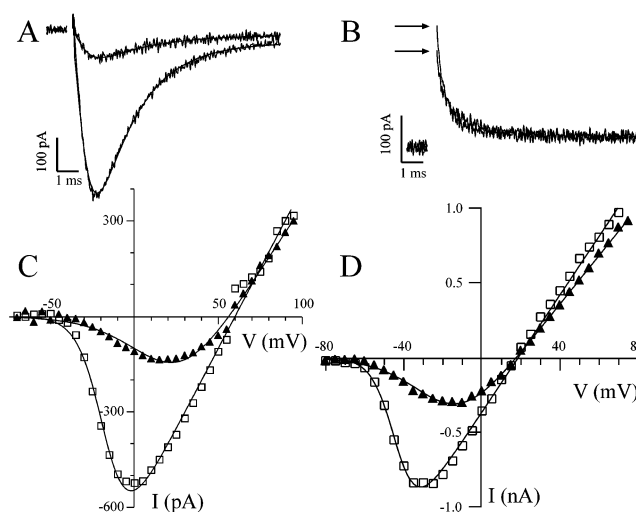

FIGURE 5: ProTx-I and ProTx-II inhibition of hNa_V 1.5 channels expressed in HEK-293 cells. Superimposed Na currents with and without ProTx-I for test potentials of −10 (A) and +95 mV (B). (C) Peak hNa_v 1.5 current plotted as a function of test potential with and without 365 nM ProTx-I (experiment depicted in panels A and B). Both curves assume a linear current−voltage relationship and are the best-fit by a Boltzmann distribution. Control (□): midpoint potential ($V_{1/2}$) = −17 mV, slope factor (k) = 7.53 mV, and maximal sodium conductance ($G_{Na,max}$) = 10.1 nS. With ProTx-I (▲): $V_{1/2}$ = +19.7 mV, k = 16.0 mV, $G_{Na,max}$ = 7.92 nS. Pipet solution (a) and bath solution (a) were used. (D) hNa_v 1.5 currents in the absence and presence of 200 nM ProTx-II at test potentials between −80 and +75 mV. Both curves assume a linear current−voltage relationship and are the best fit by a Boltzmann distribution. Control (□): $V_{0.5act}$ = −43.3 mV, k = 5.8 mV. With 200 nM ProTx-II (▲): −19.7 mV, k = 12.7 mV. Pipet solution (b) and bath solution (b) were used.

(Figure 5D). The shift in the voltage of half-maximal activation with 200 nM ProTx-II was +24 mV, similar to the shift observed with 365 nM ProTx-I. Likewise, the slope factor is increased ≈2-fold. In these experiments, no obvious change in inactivation rate was observed, unlike other peptides that effect Na_V channel gating (*1*). These effects are similar to those of hanatoxin1 on K_V 2.1 and indicate that ProTx-I and ProTx-II are gating modifier peptides.

ProTx-I was also tested on rCa_V 3.1 calcium channels (T-type) stably expressed in HEK-293 cells to determine selectivity and to obtain more insight into the mechanism of current inhibition. We examined possible effects of ProTx-I on Ca_V 3.1 channel activation by measuring tail currents after brief depolarizations to different test potentials in the absence or presence of toxin (Figure 6). At negative test potentials, such as −40 mV, 1 μM ProTx-I inhibits calcium current through rCa_V 3.1 channels by 84%. However, when pulsing to +40 mV, only a 26% decrease of the tail current amplitude was observed. Channels opened by strong depolarizations (+40 mV) activated slightly more slowly and deactivated more rapidly in the presence of ProTx-I (Figure 6A).

Channel activation curves shown in Figure 6B illustrate the voltage dependent inhibition by 1 μM ProTx-I of rCa_V 3.1 over a wide voltage range from −80 to +40 mV. Tail current amplitudes are plotted versus test pulse voltage. Resulting activation curves are well described by a single Boltzmann function with a midpoint ($V_{0.5act}$) of −32 mV and a slope (k) of 7.6 mV under control conditions. The presence of 1 μM ProTx-I in the bath solution shifts activation curves
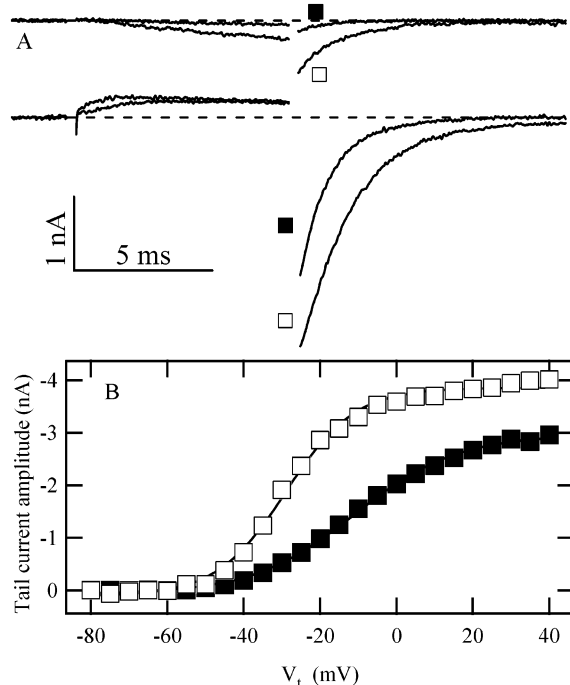
FIGURE 6: Voltage-dependent inhibition by ProTx-I of low voltage activated Ca_V 3.1 (T-type) channels expressed in HEK-293 cells. (A) Currents elicited by 8 ms depolarizations (V_t) to −40 (upper) and +40 mV (lower) and tail current measurements following repolarization to −110 mV in the absence (□) or presence (■) of 1 μM ProTx-I. B: Peak inward tail currents measured as in A at the indicated activation potential: V_t. 1 μM ProTx-I shifts current activation curves to more positive voltages and reduces the steepness of the curves. Activation curves were fitted to single Boltzmann functions with $V_{1/2}$ (control) = −32 mV, k = 7.6 and $V_{1/2}$ (1 μM ProTx-I) = −11 mV, k = 13.4.

about 20 mV to more depolarized voltages and reduces the steepness of the activation curve ($V_{0.5act}$ = −11 mV, k = 13.4 mV; Figure 6B). These results suggest that ProTx-I interferes with rCa_V 3.1 channel activation. A similar mode of action on calcium channels has been described for other peptide toxins that inhibit channel activation, such as ω-grammotoxin-SIA, ω-Aga-IVA, and kurtoxin (13, 43, 44).

For some voltage-activated ion channels, the process of channel inactivation is coupled to channel opening (45). Consequently, modulation of rCa_V 3.1 channel activation by ProTx-I also might result in changes of voltage dependent inactivation. Steady-state inactivation in the absence and presence of 365 nM and 1 μM ProTx-I was determined from tail current amplitudes. Following 10s conditioning prepulses to potentials from −110 to −40 mV and an 8 ms pulse to −10 mV, a tail current was measured at −110 mV to determine how many channels inactivated. Interestingly, ProTx-I has little to no effect on the steady-state availability of rCa_V 3.1: for control conditions, $V_{0.5inact}$ = −68 ± 1 (n = 4); in 356 nM toxin, $V_{0.5inact}$ = −73 ± 3 (n = 2); and in 1 μM toxin, $V_{0.5inact}$ = −73 ± 1 (n = 2).

Chemical Synthesis of ProTx-I and ProTx-II. To demonstrate that ProTx-I and ProTx-II are responsible for the observed biological activities of these peptides, they were chemically synthesized. After air oxidation, only one major form with the expected masses of 3827 and 3988 amu were found for ProTx-II and ProTx-I, respectively. The yield on the folding reaction was quite high at >70% for both toxins. This material was identical to native material by HPLC

analysis, and the synthetic ProTx-II coeluted with native ProTx-II on C-18 HPLC (data not shown). Native ProTx-I was not available to try coelution experiments since recent venom samples did not yield any ProTx-I.

The synthetic ProTx-II was subject to the disulfide bridge mapping protocol and gave results identical to those found with the native peptide (Figure 4). Synthetic ProTx-II was subject to NMR analysis to obtain additional evidence for the formation of the expected ICK disulfide bridges. Sequence-specific ^{1}H resonance assignments were obtained on the peptide. The analysis of the observed NOEs involving the backbone and side chain resonances from the six-half-cystine residues identified the disulfide pairings (Appendix). The NOE data are complimentary with the other lines of evidence and are compatible with the disulfide pairing shown in Figure 4.

Synthetic and native ProTx-I and ProTx-II were compared in several assay systems with multiple Na_V and rCa_V 3.1 channels to compare biological potencies. Native and synthetic ProTx-I were evaluated at concentrations between 20 and 800 nM on hNa_V 1.7 expressed in oocytes and found to have similar potencies (IC_{50} = 51 and 72 nM, respectively, Figure 7A squares). The inhibition appeared to saturate at about 80−90% when using a test potential that elicited maximal inward currents for hNa_V 1.7 (0 mV), as might be expected for a gating modifier peptide. Native ProTx-I and ProTx-II inhibited rNa_V 1.8 expressed in oocytes in a similar manner with apparent potencies of 27 and 19 nM, respectively (data not shown).

The potency of native and synthetic ProTx-II was evaluated using whole-cell voltage-clamp recordings of HEK-293 cells stably expressing hNa_V 1.5. The peak inward current obtained at −40 mV was measured in the absence or presence of various concentrations of native and synthetic ProTx-II (Figure 7A, circles). Synthetic ProTx-II yielded virtually identical results to those obtained with native toxin isolated from venom, confirming that this biological activity resides in this molecule. Block of hNa_V 1.5 by synthetic ProTx-II gave an IC_{50} value of 29 nM, very close to the 19 nM potency observed with the native ProTx-II. The native and synthetic forms were also not distinguishable in potency on hNa_V 1.7, though the high potency (80% block at 3 nM) and slow on-rates precluded more quantitative analysis.

The apparent potency of ProTx-I for inhibition of rCa_V 3.1 channels was determined using a method suggested for quantifying K_V channel inhibition by hanatoxin1 (46). To quantify the fraction of unbound channels, we measured the fraction of uninhibited tail current at weak depolarizations (−40 mV) in the presence of native and synthetic ProTx-I. The remaining tail current amplitude following test pulses was normalized and plotted against toxin concentration. IC_{50} values of 53 and 69 nM for native and synthetic ProTx-I, respectively, were obtained (Figure 7A, triangles).

Native and synthetic ProTx-II also showed similar activity in a high-throughput functional assay using hNa_V 1.7. The assay uses membrane potential-dependent redistribution of one-half of a fluorescence resonance energy transfer (FRET) dye pair to give a FRET signal which is related to Na_V channel mediated depolarization of cells in 96-well plates (37, 47). The middle left panel shows the red and blue fluorescence emission signals (normalized to one) and the time course of change in each with Na addition. The stippled
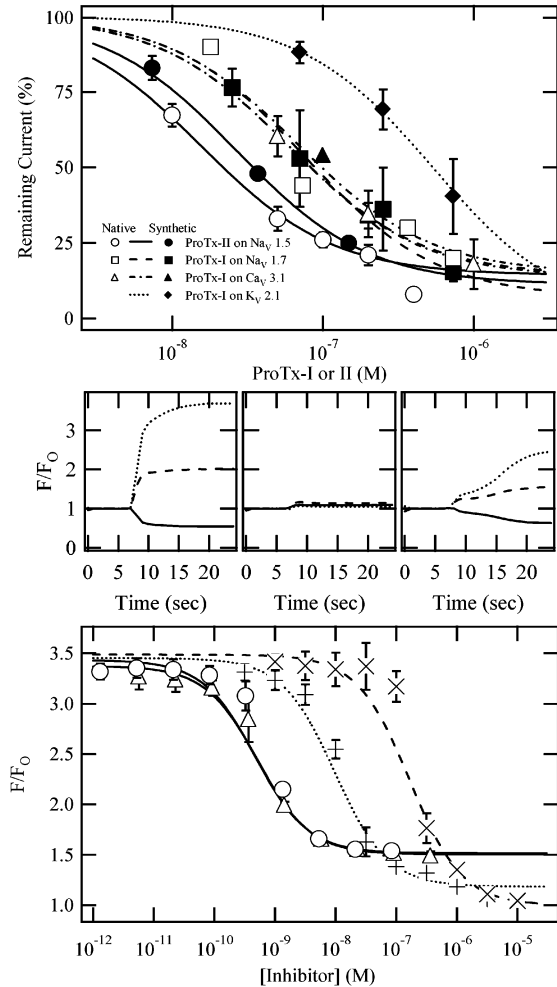
FIGURE 7: Native and synthetic ProTx-I and ProTx-II inhibit various channel types with similar potencies. Upper panel: inhibition of various currents by native (open symbols) and synthetic (filled symbols) ProTx-I & ProTx-II. Plot of remaining Na$_V$ 1.5 current ($V_t = -40$ mV, as in Figure 5D) in the presence of different concentrations of native (○) and synthetic (●) ProTx-II ($n = 2-9$) and fit to IC$_{50}$ values of 19 and 29 nM, respectively. Remaining Ca$_V$ 3.1 tail current amplitude ($V_t = -40$ mV, as in Figure 6) in the presence of the indicated concentrations of ProTx-I (▲, △). Native IC$_{50}$ = 53 nM ($n = 3-8$); synthetic IC$_{50}$ = 69 nM ($n = 1-2$). Remaining Na$_V$ 1.7 current ($V_t = 0$ mV) measured in oocytes in the presence of the indicated concentrations of native (□) and synthetic (■) ProTx-I. Native IC$_{50}$ = 51 nM ($n = 1$); synthetic IC$_{50}$ = 72 nM ($n = 2$). Remaining K$_V$ 2.1 current ($V_t = 0$ mV) measured in oocytes in the presence of the indicated concentrations of synthetic (◆) ProTx-I fit to an IC$_{50}$ = 411 nM ($n = 2$). Middle panels: fluorescence traces of representative wells showing depolarization induced change in FRET in individual wells. Left panel, control (no drug); center panel, 1 μM tetrodotoxin; right panel, 0.1 μM native ProTx-II. Individual lines are the change in red fluorescence (580 nm, solid lines), in blue fluorescence (460 nm, dashed lines), and in the blue/red FRET ratio (F/F$_0$, stippled lines). The addition of Na at 7 s caused a robust change in the red and blue fluorescence emissions in control wells and a substantial change in the FRET ratio. Lower panel: inhibition of Na$_V$ 1.7 FRET by tetrodotoxin (+), by WIN 17317−3 (X) and by native and synthetic ProTx-II (○ and △, respectively). Standard deviations of the triplicates are shown; error bars not visible are smaller than the size of symbol. The time of quantification of change in FRET was 12−15 s/1−6 s. The lines are models of potencies (Hill coefficients fixed at 1) of tetrodotoxin, 14 nM, of WIN 17317-3, 0.232 μM and 0.8 nM and 1 nM for native and synthetic ProTx-II, respectively ($n = 2$). This type of assay, with other agonist stimulation conditions has been run six times; similar potencies for native and synthetic have always been observed.

Table 2: Inhibition of Several Na$_V$ and K$_V$ Channels by ProTx-I and ProTx-II[a]

channel	% inhibition[b]	
	ProTx-I	ProTx-II
Na$_V$ 1.2	83	75
Na$_V$ 1.5	77	74
Na$_V$ 1.7	80	82
Na$_V$ 1.8	73	63
K$_V$ 1.2	6	0
K$_V$ 1.3	40	2
K$_V$ 1.5	7	−2
K$_V$ 2.1	60[c]	5

[a] The indicated Na$_V$ or K$_V$ channels were expressed in oocytes and the channel activity monitored using two-electrode voltage-clamp. The membrane potential was voltage-clamped at −80 mV, and the peak currents were measured at 0−30 mV. [b] Reduction in peak current after addition of either 730 nM ProTx-I or 460 nM ProTx-II to each channel isoform indicated. [c] Synthetic Protx-I (730 nM) was used for this value (see Figure 7A).

trace shows the change in the FRET. In the presence of 1 μM of the pore blocker, tetrodotoxin (TTX), changes in FRET were not seen (Figure 7, middle panel). In the presence of 0.25 μM native ProTx-II (Figure 7, middle right panel), changes in the FRET signal were delayed. The assay displayed the appropriate pharmacological sensitivity to tetrodotoxin and WIN 17317−3 with IC$_{50}$s of 14 nM and 232 nM, respectively, (Figure 7, lower panel, *48*). Native and synthetic ProTx-II were of similar potency, −0.8 versus 1.0 nM, respectively, consistent with the potency measured by electrophysiological techniques (74% and 89% block at 5 nM, for native and synthetic ProTx-II, respectively). If the F/F_O ratio was measured later after Na addition (22−25 s), the potency calculated decreased by a factor of 2 (data not shown), but the maximal inhibition decreased from 80% to ca. 50% (Figure 7, middle right panel). Native and synthetic ProTx-II were equipotent and less active in this assay using hNa$_V$ 1.5 cells (IC$_{50}$ of 250 nM, ca. 30% maximal inhibition, data not shown). This high throughput assay with hNa$_V$ 1.7 cells was used to support the purification of ProTx-II from venom in the most recent purification.

The selectivity of both ProTx-I and ProTx-II was tested on several other Na$_V$ and K$_V$ channels expressed in oocytes (Table 2). ProTx-I and ProTx-II blocked Na$_V$ 1.2, Na$_V$ 1.5, Na$_V$ 1.7, and Na$_V$ 1.8 by about 80% at test concentrations of 730 and 460 nM, respectively. These results suggest that neither peptide shows a large degree of isoform selectivity. However, the rate at which each isoform recovered from ProTx-II inhibition varied from less than 2 min (Figure 1) to more than 20 min (data not shown). In fact, hNa$_V$1.7 showed no recovery during 20 min of washout after ProTx-II exposure. In contrast, ProTx-I did not show significant differences in recovery rates among the four Na$_V$ isoforms tested (data not shown).

Since both peptides have some homology with hanatoxin1, which blocks K$_V$ 2.1 channels, we also tested the potency of ProTx-I and ProTx-II at a single high concentration on K$_V$ 2.1 and three K$_V$ 1.X channels expressed in oocytes (Table 2). ProTx-I showed partial block of K$_V$ 1.3 (40% at 730 nM); no significant block was seen with K$_V$ 1.2 or K$_V$ 1.5, and ProTx-II showed no block of any of the K$_V$ 1.X channels tested in oocytes. However, ProTx-I, which is 57% identical to hanatoxin1, inhibited K$_V$ 2.1 by 60% at 730 nM

and displayed an IC$_{50}$ of 411 nM (Figure 7A, diamonds). ProTx-II only inhibited 5% of the K$_V$ 2.1 current at 460 nM.

DISCUSSION

We have purified and characterized two peptides, ProTx-I and ProTx-II, that are abundant in the venom of the tarantula *Thrixopelma pruriens*. These toxins are potent inhibitors of both TTX-sensitive and TTX-resistant sodium channels (Na$_V$ 1.2, 1.5, 1.7, and 1.8); they inhibited all Na$_V$ channels tested. Although a variety of natural products target voltage-gated sodium channels (*49*), these two spider toxins are the first known agents that inhibit Na$_V$ channel activation. Inhibition of activation is well-known for voltage-gated K and Ca channels, and ProTx-I and ProTx-II share striking structural and functional similarities to other ICK gating-modifier toxins. Both peptides belong to the class of ICK peptides that have 6 half-cystine residues that form 3 disulfide bonds by forming bonds from the first, second and third cys residues to the fourth, fifth, and sixth cys residues, respectively; these disulfide bonds result in a rigid peptide backbone that forms four loops (*10*). Although both toxins share a similar structural backbone, have similar effects on Na$_V$ channel gating, and bind to Na$_V$ 1.8 with similar affinity, they are almost completely dissimilar at all nonhalf-cystine residues: only W$_5$, V$_{20}$, and W$_{24}$ (W$_{27}$ in ProTx-I) are identical between the 2 toxins. This very limited homology may suggest that these residues could define the active face of both toxins, as discussed below.

ProTx-I also inhibits the activation of Ca$_V$ 3.1 channels. Such promiscuous activity raises concerns that the isolated peptide preparation is not pure enough. For this reason, we have taken great care to ensure that the results were obtained with purified toxins. By three metrics (MS, protein sequencing, and HPLC analysis) the material was estimated to be >97% pure. ProTx-I is not the only toxin that modifies both Na$_V$ and Ca$_V$ channels. At least two other toxins have been shown to modify both channel types; the α-scorpion-toxin-like peptide, kurtoxin (*44, 50*), and the cone snail peptide, conotoxin MrVIB (*51*). Small molecule inhibitors such as phenytoin and lifarizine can inhibit both Na$_V$ and Ca$_V$ channels as well (*52*). In addition, preliminary experiments with ProTx-II reveal that it can modify some Ca$_V$ 1.X and Ca$_V$ 3.X channels (*21, 22*); these studies are ongoing. This ability to interact with multiple ion channel families is more common among state-dependent inhibitors as compared to pore-blocking inhibitors.

To rule out the possibility that a very potent minor contaminant was present, we prepared synthetic ProTx-II and demonstrated that it has the same disulfide bridging pattern and biological activity as the native ProTx-II. The folding reaction yield was fortunately quite high at 77%. The native and synthetic ProTx-II were shown to be equipotent in two functional assays: by electrophysiological analysis and a Na$_V$ channel mediated-membrane depolarization assay (VIPR). The VIPR assay is a high throughput fluorescence assay that can measure membrane depolarization induced by Na influx through agonist-stimulated Na$_V$ channels. The assay is robust with a high signal-to-noise ratio (Z-factors of 0.80 and 0.79 for the two plates shown, *53*). TTX and WIN 17317-3 completely blocked the signal in a dose-dependent manner, with potencies similar to those reported for these compounds

inhibiting ^{22}Na uptake through Na$_V$ 1.2 expressing cells (*48*). ProTx-II decreased the initial response to Na addition by ca. 80%, but with time, the cells did depolarize further. The apparent reversal of Na$_V$ channel inhibition may be due to the inability of ProTx-II to block at depolarized potentials (as seen in Figures 5 and 6). Since ProTx-II inhibits channel activity by modifying the voltage dependence of activation, even in the presence of ProTx-II, a small depolarization could cause some Na$_V$ channels to open, triggering further depolarization and additional channel opening. Na influx at any given ProTx-II concentration would depend on the microscopic rate constants of channel gating, agonist activation, and peptide inhibition. The complex nonequilibrium condition that exists in the VIPR assay may explain why ProTx-II block was decreased with time in the assay.

ProTx-II was chosen for disulfide bridge analysis, as it does not conform exactly to the ICK definition. ProTx-II has only three residues between the 5th and 6th half-cystines, whereas the ICK motif is defined as 4−13 residues between those half-cystines (*11*). Huwentoxin-II, another peptide isolated from a spider venom, also has six half-cystine residues with a spacing that does not conform to the ICK motif, and it does not form a cystine knot structure (*54, 55*). By physical separation, the disulfide between C$_9$ and C$_{21}$ of ProTx-II was proven to exist: a peak with the predicted amino acid sequence and mass that was reductant-sensitive was isolated. Since C$_{15}$ and C$_{16}$ could not be enzymatically cleaved, the other two disulfide pairs were not physically separated. However, we did isolate a disulfide-linked tripeptide that contained C$_2$, C$_{15}$, C$_{16}$, and C$_{25}$. Therefore, C$_2$ and C$_{25}$ must bridge to C$_{15}$C$_{16}$. Three lines of evidence that C$_2$ bridges to C$_{16}$ (and therefore C$_{15}$ bridges to C$_{25}$) were found: sequencing, MS/MS, and NOESY. Taken together, the data strongly point to the disulfide bridging pattern for ProTx-II as being that of an ICK protein, and thus the consensus definition of ICK proteins must be altered from 4 to 13 residues spacing to 3−13 residues between the 5th and 6th cys residues (*11*).

Since ProTx-I and hanatoxin1 have similar potencies at inhibiting K$_V$ 2.1 (Figure 7, top panel, *41*) and the same half-cystine spacing and extensive sequence identity, it is reasonable to model the structure of ProTx-I assuming a three-dimensional structure similar to that of hanatoxin1. The structure of hanatoxin1 has been determined by NMR (*39*) and is shown in Figure 8. Also shown are the corresponding calculated backbone structures for ProTx-I and ProTx-II assuming a conformation similar to that of hanatoxin1; structures were developed using MOE (*56*). In the downward direction, we have shown the location of a group of hydrophobic residues (green side chains) that form a hydrophobic patch similar to that observed in the hanatoxin NMR structure. These include W$_5$ and W$_{27}$ (W$_{24}$) that are conserved between ProTx-I and ProTx-II but are not in hanatoxin1. The third conserved residue, V20, is not highlighted and is located behind the plane shown in Figure 8. If all three of these residues are important, then a large part of the surface area of these peptides is involved in binding to their receptor sites. (This might be consistent with a binding site located deep within a crevice of the channel.) There are also from 6 to 10 charged residues in all three peptides (blue = positive, red = negative), and their distribution, which is substantially different between the three
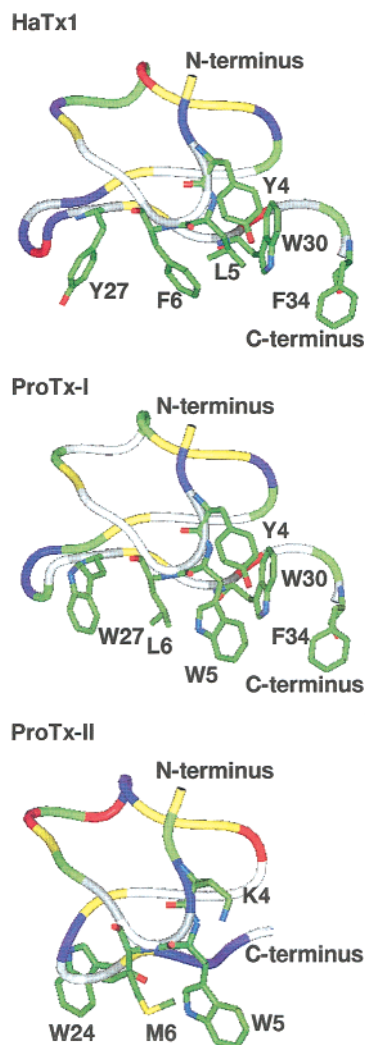
FIGURE 8: Modeling of the ProTx-I and ProTx-II structure and comparison to hanatoxin1. The ProTx-I and ProTx-II homology models and the hanatoxin1 (HaTx1) structure derived from NMR experiments (pdb code 1D1H) are shown as indicated. The ProTx homology models were generated based on the hanatoxin1 NMR structure, using the software MOE (*56*). Blue represents the positively charged residues Lys and Arg; red is for negatively charged residues Asp and Glu; yellow shows Cys residues; green is for polar residues Ser, Thr, His, Asn, and Gln; white represents nonpolar residues Met, Ala, Val, Leu, Ile, Pro, and Gly and aromatic residues Phe, Tyr, and Trp (double bonds are not displayed for clarity). Green indicates the residues for which the side chains are shown.

peptides, will likely influence binding, and may play a role in function as well.

The similarities with hanatoxin1 suggest that ProTx-I and ProTx-II bind to an S3−S4 linker of voltage-gated ion channels and thereby inhibit channel activation (*16*). Similar inhibition of Ca$_V$ channel activation is observed with the spider toxins ω-Agatoxin-IVA, ω-grammotoxin-SIA, SNX-482, and the scorpion toxin kurtoxin (*19*, *43*, *44*, *50*, *57*). All of these toxins are thought to bind to the channel's voltage-sensing domain and presumably inhibit the movement of S4 segments. The movement of S4 participates in transducing membrane depolarization into channel activation (*45*). Likewise, the α-scorpion toxins and some sea anemone toxins bind to Na$_V$ channels within the voltage-sensing portion of domain IV and inhibit gating charge movement

(*5*, *58*). These toxins modify channel gating by slowing channel inactivation apparently by disrupting the coupling between channel opening and inactivation. β-Scorpion toxins bind to the voltage-sensing portion of domain II and cause a hyperpolarizing shift in both activation and inactivation, evidently by trapping the activation gate in the open configuration (*8*). It will be interesting to locate the part of the voltage-sensor(s) that bind ProTx-I and ProTx-II since they apparently hinder the activation process without dramatic affects on the inactivation gate. This mechanism is unlike the other gating modifier toxins of the Na$_V$ channel, but is similar to the gating modifications caused by ω-Aga-toxin-IVA which has been mapped to the voltage sensor in domain IV of α$_{1A}$ Ca$_V$ channels (*14*).

Given that ProTx-I and ProTx-II inhibit both Na$_V$ channels and T-type Ca$_V$ channels, it will be of interest to determine how conserved the binding domains are in these two channels. It may be that these peptides interact with domain II or IV (Na$_V$ channel toxin sites 4 and 3, respectively) or some other voltage-sensing domain on the two channel types. Further, it may be a different domain in the two channel families. Finally, each toxin may interact with different voltage sensor domains on the same channel. Future experiments involving co-application of ProTx-I and ProTx-II along with other gating modifiers should help to answer these questions (*22*). Given these numerous possibilities, it is unproductive to try to predict on the basis of sequence homology where the binding sites are located. However, the mapping of α-scorpion toxins, ω-Agatoxin-IVA, and hana-toxin1 in Na$_V$, Ca$_V$, and K$_V$ channels has revealed a "hot spot" for the binding of gating modifiers in the S3−S4 linker (*5*, *14*, *19*). Alignment of this region in all four domains of Na$_V$ 1.5, 1.7, 1.8, and Ca$_V$ 3.1 channels reveals considerable homology (40−68%). Domain II (68%) and domain IV (64%) have a larger number of conserved residues compared to domains I (40%) and III (46%). Of course, there may be very few critical residues forming the binding site on the channels that are similar or identical between all four channels, but it will require site-directed mutagenesis studies to resolve that question. Hopefully, the ability to produce large amounts of synthetic ProTx-I and ProTx-II will help with these studies.

ACKNOWLEDGMENTS

APPENDIX

The synthetic folded ProTx-II was subject to analysis by NMR. Sequence-specific ^{1}H resonance assignments were obtained on the peptide. The analysis of the observed NOEs involving the backbone and side chain resonances from the six-half-cystine residues identified the disulfide pairings.

There was strong evidence for the three disulfide pairings, $C_{16}-C_2$, $C_{21}-C_9$, and $C_{15}-C_{25}$ found in the NOESY spectrum of the peptide. NOEs were identified between the C_{16} Hα-resonance and both C_2 Hβ-resonances. There is also an NOE observed between the C_{16} amide NH-resonance and one C_2 Hβ-resonance (C_2-C_{16}). The C_9-C_{21} disulfide pairing was identified by two NOEs. There is an NOE observed between one C_{21} Hβ-resonance and a C_9 Hβ-resonance. An NOE was also observed between the C_9 Hα-resonance and one C_{21} Hβ-resonance. The $C_{15}-C_{25}$ disulfide pairing was also identified by two NOEs. There is an NOE observed between one of the C_{15} Hβ-resonances and one of the C_{25} Hβ-resonances. There is also an NOE observed between the C_{15} Hα-resonance and a C_{25} Hβ-resonance. The NOE data strongly suggest that the three disulfide pairings are as shown (Figure 4). However, because C_{15} and C_{16} are next to each other in the peptide primary sequence, some of the observed NOEs involving these residues may be due to the tertiary fold of the peptide (long-range NOEs) and not the result of a disulfide bridge.

REFERENCES

1. Cestele, S., and Catterall, W. A. (2000) Molecular Mechanisms of Neurotoxin Action on Voltage-Gated Sodium Channels, *Biochimie 82*, 883−892.

2. Safo, P., Rosenbaum, T., Shcherbatko, A., Choi, D. Y., Han, E., Toledo-Aral, J. J., Olivera, B. M., Brehm, P., and Mandel, G. (2000) Distinction among Neuronal Subtypes of Voltage-Activated Sodium Channels by μ-Conotoxin PIIIA, *J. Neurosci. 20*, 76−80.

3. Penzotti, J. L., Lipkind, G., Fozzard, H. A., and Dudley, S. C., Jr. (2001) Specific Neosaxitoxin Interactions with the Na⁺ Channel Outer Vestibule Determined by Mutant Cycle Analysis, *Biophys. J. 80*, 698−706.

4. Cruz, L., Gray, W., Olivera, B., Zeikus, R., Kerr, L., Yoshikami, D., and Moczydlowski, E. (1985) *Conus Geographus* Toxins That Discriminate between Neuronal and Muscle Sodium Channels, *J. Biol. Chem. 260*, 9280−9288.

5. Rogers, J. C., Qu, Y., Tanada, T. N., Scheuer, T., and Catterall, W. A. (1996) Molecular Determinants of High Affinity Binding of α-Scorpion Toxin and Sea Anemone Toxin in the S3−S4 Extracellular Loop in Domain IV of the Na⁺ Channel α Subunit, *J. Biol. Chem. 271*, 15950−15962.

6. Benzinger, G. R., Kyle, J. W., Blumenthal, K. M., and Hanck, D. A. (1998) A Specific Interaction between the Cardiac Sodium Channel and Site-3 Toxin Anthopleurin B, *J. Biol. Chem. 273*, 80−84.

7. Shon, K. J., Hasson, A., Spira, M., Cruz, L., Gray, W., and Olivera, B. (1994) δ-Conotoxin GmVIA, a Novel Peptide from the Venom of *Conus gloriamaris*, *Biochemistry 33*, 11420−11425.

8. Cestele, S., Qu, Y., Rogers, J. C., Rochat, H., Scheuer, T., and Catterall, W. A. (1998) Voltage Sensor-Trapping: Enhanced Activation of Sodium Channels by β-Scorpion Toxin Bound to the S3−S4 Loop in Domain II, *Neuron 21*, 919−931.

9. Escoubas, P., Diochot, S., and Corzo, G. (2000) Structure and Pharmacology of Spider Venom Neurotoxins, *Biochimie 82*, 893−907.

10. Norton, R. S., and Pallaghy, P. K. (1998) The Cystine Knot Structure of Ion Channel Toxins and Related Polypeptides, *Toxicon 36*, 1573−1583.

11. Craik, D. J., Daly, N. L., and Waine, C. (2001) The Cystine Knot Motif in Toxins and Implications for Drug Design, *Toxicon 39*, 43−60.

12. Harrison, P. M., and Sternberg, M. J. (1996) The Disulphide β-Cross: From Cystine Geometry and Clustering to Classification of Small Disulphide-Rich Protein Folds, *J. Mol. Biol. 264*, 603−623.

13. McDonough, S. I., Mintz, I. M., and Bean, B. P. (1997) Alteration of P-Type Calcium Channel Gating by the Spider Toxin ω-Aga-IVA, *Biophys. J. 72*, 2117−2128.

14. Winterfield, J. R., and Swartz, K. J. (2000) A Hot Spot for the Interaction of Gating Modifier Toxins with Voltage-Dependent Ion Channels, *J. Gen. Physiol. 116*, 637−644.

15. Hans, M., Urrutia, A., Deal, C., Brust, P. F., Stauderman, K., Ellis, S. B., Harpold, M. M., Johnson, E. C., and Williams, M. E. (1999) Structural Elements in Domain IV That Influence Biophysical and Pharmacological Properties of Human α$_{1A}$-Containing High-Voltage-Activated Calcium Channels, *Biophys. J. 76*, 1384−1400.

16. Swartz, K. J., and MacKinnon, R. (1997) Mapping the Receptor Site for Hanatoxin, a Gating Modifier of Voltage-Dependent K⁺ Channels, *Neuron 18*, 675−682.

17. Bourinet, E., Soong, T. W., Sutton, K., Slaymaker, S., Mathews, E., Monteil, A., Zamponi, G. W., Nargeot, J., and Snutch, T. P. (1999) Splicing of α$_{1A}$ Subunit Gene Generates Phenotypic Variants of P- and Q-Type Calcium Channels, *Nat. Neurosci. 2*, 407−415.

18. Escoubas, P., Diochot, S., Celerier, M. L., Nakajima, T., and Lazdunski, M. (2002) Novel Tarantula Toxins for Subtypes of Voltage-Dependent Potassium Channels in the K$_v$2 and K$_v$4 Subfamilies, *Mol. Pharmacol. 62*, 48−57.

19. Li-Smerin, Y., and Swartz, K. J. (1998) Gating Modifier Toxins Reveal a Conserved Structural Motif in Voltage-Gated Ca²⁺ and K⁺ Channels, *Proc. Natl. Acad. Sci. U.S.A. 95*, 8585−8589.

20. Middleton, R., Cohen, C. J., Dai, G., Kohler, M., Liu, J., Brochu, R., Hwang, C., Warren, V. A., and Smith, M. M. (1998) A Spider Toxin That Inhibits TTX-Resistant and Other Mammalian Sodium Channels, *Biophys. J. 74*, A81.

21. Kraus, R. L., Warren, V. A., Smith, M. M., Middleton, R. E., and Cohen, C. J. (2000) Modulation of α$_{1G}$ and α$_{1C}$ Calcium Channels by the Spider Toxin ProTx-II, *Soc. Neurosci. Abstr. 26*, 623.

22. Kraus, R. L., Warren, V. A., Smith, M. M., Middleton, R. E., Blumenthal, K. M., and Cohen, C. J. (2002) A Spider Toxin That Inhibits Activation of Voltage-Gated Sodium Channels, *Biophys. J. 82*, 85a.

23. Schmidt, G. (1998) Die Chilenischen Vogelspinnen Der Gattungen *Grammostola Simon*, 1892, *Paraphysa Simon*, 1892, *Euathlus Ausserer*, 1875 Und *Thrixopelma Schmidt*, 1994 (Araneae: *Mygalomorphae*: *Theraphosidae*: *Theraphosinae*) Mit Beschreibung Einer Neuen *Thrixoplema*-Spezies, *Arthropoda 6*, 3−10.

24. Ertel, E. A., Warren, V. A., Adams, M. E., Griffin, P. R., Cohen, C. J., and Smith, M. M. (1994) Type III ω-Agatoxins: A Family of Probes for Similar Binding Sites on L- and N-Type Calcium Channels, *Biochemistry 33*, 5098−5108.

25. Garsky, V. M., Lumma, P. K., Freidinger, R. M., Smith, M. M., and Cohen, C. J. (1995) The Total Chemical Synthesis of μ-Agatoxin-IV: A Spider Toxin Selective for Insect Na Channels, in *Peptides 1994* (Maia, H. L. S., Ed.) pp 375−376, ESCOM Science Publishers B.V., Leiden.

26. Braunschweiler, L., and Ernst, R. R. (1983) Coherence Transfer by Isotropic Mixing: Application to Proton Correlation Spectroscopy, *J. Magn. Reson. 53*, 521−528.

27. Bax, A., and Davis, D. G. (1985) MLEV-17-Based Two-Dimensional Homonuclear Magnetization Transfer Spectroscopy, *J. Magn. Reson. 65*, 355−360.

28. Jeener, J., Meier, M. H., Bachmann, P., and Ernst, R. R. (1979) Investigation of Exchange Processes by Two-Dimensional NMR Spectroscopy, *J. Chem. Phys. 71*, 4546−4553.

29. Wuthrich, K. (1986) *NMR of Proteins and Nucleic Acids*, John Wiley & Sons, New York.

30. States, D. J., Haberkorn, R. A., and Ruben, D. J. (1982) A Two-Dimensional Nuclear Overhauser Experiment with Pure Absorption Phase in Four Quadrants, *J. Magn. Reson. 48*, 286−292.

31. Levitt, M. H., Freeman, R., and Frenkiel, T. (1982) Broadband Heteronuclear Decoupling, *J. Magn. Reson. 47*, 328−330.

32. Akopian, A. N., Sivilotti, L., and Wood, J. N. (1996) A Tetrodotoxin-Resistant Voltage-Gated Sodium Channel Expressed by Sensory Neurons, *Nature 379*, 257−262.

33. Goldin, A. L. (1991) Expression of Ion Channels by Injection of mRNA into Xenopus Oocytes, *Methods Cell Biol. 36*, 487−509.

34. Hartmann, H. A., Tiedeman, A. A., Chen, S. F., Brown, A. M., and Kirsch, G. E. (1994) Effects of III−IV Linker Mutations on Human Heart Na⁺ Channel Inactivation Gating, *Circ. Res. 75*, 114−122.

35. Klugbauer, N., Lacinova, L., Flockerzi, V., and Hofmann, F. (1995) Structure and Functional Expression of a New Member of the Tetrodotoxin-Sensitive Voltage-Activated Sodium Channel Family from Human Neuroendocrine Cells, *EMBO J. 14*, 1084−1090.

36. Perez-Reyes, E., Cribbs, L. L., Daud, A., Lacerda, A. E., Barclay, J., Williamson, M. P., Fox, M., Rees, M., and Lee, J. H. (1998)

Molecular Characterization of a Neuronal Low-Voltage-Activated T-Type Calcium Channel, *Nature 391*, 896−900.

37. Gonzalez, J. E., and Tsien, R. Y. (1997) Improved Indicators of Cell Membrane Potential That Use Fluorescence Resonance Energy Transfer, *Chem. Biol. 4*, 269−277.

38. Gonzalez, J. E., and Tsien, R. Y. (1995) Voltage Sensing by Fluorescence Resonance Energy Transfer in Single Cells, *Biophys. J. 69*, 1272−1280.

39. Takahashi, H., Kim, J. I., Min, H. J., Sato, K., Swartz, K. J., and Shimada, I. (2000) Solution Structure of Hanatoxin1, a Gating Modifier of Voltage-Dependent K$^+$ Channels: Common Surface Features of Gating Modifier Toxins, *J. Mol. Biol. 297*, 771−780.

40. Liang, S. P., Zhang, D. Y., Pan, X., Chen, Q., and Zhou, P. A. (1993) Properties and Amino Acid Sequence of Huwentoxin-I, a Neurotoxin Purified from the Venom of the Chinese Bird Spider *Selenocosmia huwena*, *Toxicon 31*, 969−978.

41. Swartz, K. J., and MacKinnon, R. (1995) An Inhibitor of the K$_v$2.1 Potassium Channel Isolated from the Venom of a Chilean Tarantula, *Neuron 15*, 941−949.

42. Jones, M. D., Patterson, S. D., and Lu, H. S. (1998) Determination of Disulfide Bonds in Highly Bridged Disulfide-Linked Peptides by Matrix-Assisted Laser Desorption/Ionization Mass Spectrometry with Postsource Decay, *Anal. Chem. 70*, 136−143.

43. McDonough, S. I., Lampe, R. A., Keith, R. A., and Bean, B. P. (1997) Voltage-Dependent Inhibition of N- and P-Type Calcium Channels by the Peptide Toxin ω-Grammotoxin-SIA, *Mol. Pharmacol. 52*, 1095−1104.

44. Chuang, R. S. I., Jaffe, H., Cribbs, L., Perez-Reyes, E., and Swartz, K. J. (1998) Inhibition of T-Type Voltage-Gated Calcium Channels by a New Scorpion Toxin, *Nat. Neurosci. 1*, 668−674.

45. Bezanilla, F. (2000) The Voltage Sensor in Voltage-Dependent Ion Channels, *Physiol. Rev. 80*, 555−592.

46. Swartz, K. J., and MacKinnon, R. (1997) Hanatoxin Modifies the Gating of a Voltage-Dependent K$^+$ Channel through Multiple Binding Sites, *Neuron 18*, 665−673.

47. Gonzalez, J. E., and Negulescu, P. A. (1998) Intracellular Detection Assays for High-Throughput Screening, *Curr. Opin. Biotechnol. 9*, 624−631.

48. Wanner, S. G., Glossmann, H., Knaus, H. G., Baker, R., Parsons, W., Rupprecht, K. M., Brochu, R., Cohen, C. J., Schmalhofer, W., Smith, M., Warren, V., Garcia, M. L., and Kaczorowski, G. J. (1999) WIN 17317−3, a New High-Affinity Probe for Voltage-Gated Sodium Channels, *Biochemistry 38*, 11137−11146.

49. Catterall, W. A. (1992) Cellular and Molecular Biology of Voltage-Gated Sodium Channels, *Physiol. Rev. 72*, S15−S48.

50. Sidach, S., and Mintz, I. (2002) Kurtoxin, a Gating Modifier of Neuronal High- and Low-Threshold Ca Channels, *J. Neurosci. 22*, 2023−2034.

51. Fainzilber, M., van der Schors, R., Lodder, J. C., Li, K. W., Geraerts, W. P. M., and Kits, K. S. (1995) New Sodium Channel Bocking Conotoxins Also Affect Calcium Currents in *Lymnaea* Neurons, *Biochemistry 34*, 5364−5371.

52. Spedding, M., Kenny, B., and Chatelain, P. (1995) New Drug Binding Sites in Ca^{2+} Channels, *Trends Pharmacol. Sci. 16*, 139−142.

53. Zhang, J. H., Chung, T. D., and Oldenburg, K. R. (1999) A Simple Statistical Parameter for Use in Evaluation and Validation of High Throughput Screening Assays, *J. Biomol. Screen 4*, 67−73.

54. Shu, Q., Lu, S.-Y., Gu, X.-C., and Liang, S.-P. (2002) The Structure of Spider Toxin Huwentoxin-II with Unique Disulfide Linkage: Evidence for Structural Evolution, *Protein Sci. 11*, 245−252.

55. Shu, Q., Huang, R., and Liang, S. (2001) Assignment of the Disulfide Bonds of Huwentoxin-II by Edman Degradation Sequencing and Stepwise Thiol Modification, *Eur. J. Biochem. 268*, 2301−2307.

56. Chemical Computing Group Inc. (2002) *Molecular Operating Environment (MOE)*, version 2002.03, Montreal, Canada.

57. Bourinet, E., Stotz, S. C., Spaetgens, R. L., Dayanithi, G., Lemos, J., Nargeot, J., and Zamponi, G. W. (2001) Interaction of SNX482 with Domains III and IV Inhibits Activation Gating of α$_{1E}$ (Ca$_v$2.3) Calcium Channels, *Biophys. J. 81*, 79−88.

58. Sheets, M. F., and Hanck, D. A. (1995) Voltage-Dependent Open-State Inactivation of Cardiac Sodium Channels: Gating Current Studies with Anthopleurin-a Toxin, *J. Gen. Physiol. 106*, 617−640.